INTERNATIONAL JOURNAL OF HYDROGEN ENERGY 38 (2013) 7382–7393

Available online at www.sciencedirect.com

SciVerse ScienceDirect

journal homepage: www.elsevier.com/locate/he

High-purity hydrogen gas from the reaction between BOF steel slag and water in the 473–673 K range

Benjamin Malvoisin [a,*], Fabrice Brunet [a], Julie Carlut [b], German Montes-Hernandez [a], Nathaniel Findling [a], Martine Lanson [a], Olivier Vidal [a], Jean-Yves Bottero [c], Bruno Goffé [c]

[a] ISTerre, Maison des Géosciences, Université de Grenoble I, CNRS, Grenoble, France
[b] Laboratoire de Géosciences Marines, Institut de Physique du Globe de Paris, Sorbonne Paris Cité, Univ Paris Diderot, UMR 7154 CNRS, F-75005 Paris, France
[c] CEREGE, Universités Aix-Marseille-I et III, CNRS, Aix-en-Provence, France

ARTICLE INFO

Article history:
Received 13 December 2012
Received in revised form
29 March 2013
Accepted 30 March 2013
Available online 3 May 2013

Keywords:
Hydrogen production
High-purity gas
Low temperature process
BOF steel slag
Hydrothermal experiments
CO_2 sequestration

ABSTRACT

A novel method for producing hydrogen with water and BOF steel slag was developed. The steel slag was reacted with water during 2–57 days at 50 MPa for temperatures ranging from 473 to 673 K. The quantitative evolution of the slag and gas compositions indicated that the main H_2 producing reaction is:

$$3FeO + H_2O \rightarrow Fe_3O_4 + H_2$$

At 523 K, approximately 5 NL of H_2 per kg of slag were produced in 3 days. The reaction rate was only 1.5 times faster when the slag was crushed down to an initial particle size below 50 μm. The H_2 production has been also tested on slags carbonated beforehand at 0.142 ± 0.002 kg of CO_2 per kg of slag. The reaction was found to be thermally activated. A high purity hydrogen (99.995%) is produced with non-carbonated steel slag below 573 K whereas CH_4 production was measured in all the other experiments.

1. Introduction

Hydrogen is a promising energy vector for two reasons: 1) after radioactive substances, it is the fuel with the highest specific energy (above 120 MJ/kg); 2) water is the main by-product in hydrogen fuel cell or during combustion. However, nowadays, 98% of the hydrogen is produced by fossil fuel reforming, a high temperature process which is energy consuming and produces greenhouse gases [1]. Consequently, other processes of H_2 production are investigated in order to make hydrogen a renewable energy vector.

The steam–iron process is the oldest route for producing hydrogen [2]. It is a cyclic process in which iron oxide (typically, magnetite, Fe_3O_4) is reduced (stage I) and re-oxidized (stage II) at temperatures ranging from 873 to 1173 K. Iron reduction is achieved with a reducing gas (generally, a gas mixture of H_2 and CO produced by coal gasification) which reacts with magnetite to form wüstite (FeO) and/or iron metal (Fe). This reduced material is then oxidized back with steam to produce high-purity H_2 and magnetite [3,4].

High-tonnage carbon steel production generally consists in a first step of the reduction of the iron ore with a reducing

* *Corresponding author*. Present address: ISTerre, Maison des Géosciences BP 53, 38041 Grenoble cedex 9, France. Tel.: +33 666549074.
E-mail address: benjamin.malvoisin@ujf-grenoble.fr (B. Malvoisin).
0360-3199/$ – see front matter
http://dx.doi.org/10.1016/j.ijhydene.2013.03.163

agent such as coke, in a blast furnace. In a later step, removal of carbon is achieved in a basic oxygen furnace (BOF) by blowing pure oxygen onto the molten metal (oxidation to CO and CO_2). This process produces slags (BOF slags) as by-products generally used as road ballast or as land filler. BOF steel slags do contain iron as a main constituent, mainly in the form of FeO (wüstite, [5]). Like in stage II of the steam–iron process, it has been shown that H_2 can be directly produced during the steel-making operations by oxidizing the slags at ~1873 K with steam [6–8]. However, compared to the steam iron, this process does not produce hydrogen of high purity since CO, CO_2 and CH_4 gases are also present.

As a possible alternative, we propose here to study experimentally the high-purity H_2-producing potential of BOF steel slags oxidized with water at low temperature (below 750 K). The role of temperature, pH and crushing was investigated; these three parameters are expected to influence the wüstite oxidation kinetics and, thus, the hydrogen production kinetics.

The presence of calcium oxide and hydroxide imposes a high pH to water when contacted with BOF slags [9]. On the other hand, these two calcium-bearing phases are easily carbonated at room temperature. Carbonation allows, at the same time, to reduce the pH [9,10] and to sequester up to 0.270 kg of CO_2 per kg of BOF steel slag [9,11]. Therefore, the effect of pH lowering on H_2 purity and production has been tested here by carbonating the BOF slag beforehand. Obviously, the consecutive use of BOF slag for CO_2 sequestration and hydrogen production is tested by this mean.

2. Materials and methods

2.1. Materials

A Basic Oxygen Furnace (BOF) steel slag was sampled by [5] and used here as a starting material. The BOF steel slag was crushed for 10 min in a mortar grinder (Retsch® RM 100) into a powder with a particle size ranging from below 1 μm to 50 μm, referred to as CBOF in the following. Crushing allows to both increase the reactive surface area and homogenize the starting material. Major and minor element composition and iron speciation were previously determined by ICP-OES, X-ray diffraction, SEM and EXAFS [5,12–14]. The major element composition of the BOF slag is: CaO (44.7 wt.%), FeO (20.58 wt.%), Fe_2O_3 (3.16 wt.%), Fe (2.7 wt.%), SiO_2 (7.6 wt.%), MnO (2.86 wt.%), MgO (4.9 wt.%), Al_2O_3 (1.2 wt.%) and P_2O_5 (1.61 wt.%).

2.2. Experiments

2.2.1. Carbonation procedure

The steel slag was reacted with CO_2 following the procedure described in [10]. Twenty grams of the crushed steel slag (CBOF) were loaded in a 2 L hastelloy PARR® autoclave together with 1 L of de-ionized water (resistivity of 18.2 MΩ cm). The experiment was conducted at room temperature (296 ± 1 K) for 6 days under constant stirring. After dispersion of the BOF steel slag into water, CO_2 was injected in the reactor to reach an initial pressure of 20 bar. The pressure drop (P_{drop}) associated with both CO_2 dissolution in water and CO_2 sequestration in carbonate minerals was recorded as a function of time until pressure stabilized [10] have shown that the Ca concentration in water has little impact on the measured pressure drop associated with CO_2 dissolution (P_{diss}). Consequently, P_{diss} was measured with the same set-up but without the slag sample, i.e. pumping CO_2 in a vessel only filled with de-ionized water. The pressure drop associated with CO_2 sequestration (P_{seq}) was estimated by subtracting P_{diss} to P_{drop}. CO_2 sequestration was also quantified by thermogravimetric analyses (TGA) using a TGA/SDTA 851[e] Mettler Toledo instrument. About 10 mg of powder (±0.1 μg) were heated from 303 to 1473 K (±0.25 K) at a rate of 10 K/min in N_2.

At the end of the carbonation experiments, the solid fraction was separated by centrifugation (15 min at 13,000 rpm) and then dried during 48 h at 353 K. The carbonation product, referred to as CARBOF in the following, was used in further hydrogen production experiments.

The native pH of CBOF and CARBOF powders was determined at 298 K at the end of the carbonation stage for CARBOF and after its stabilization in water with a water to rock ratio of 50 (identical to the one of the carbonation experiment) for CBOF.

2.2.2. Hydrogen production experiments

A total of 32 experiments was carried out (see Table 1 for details). BOF, CBOF or CARBOF powders were loaded in 2–3 cm length gold tube (4.0 mm outer diameter and 3.6 mm inner diameter) with de-ionized water (resistivity of 18.2 MΩ cm) in a water to solid mass ratio ranging from 0.15 to 5.6. The capsules were welded shut and placed in horizontal cold-seal pressure vessels. Run temperatures, ranging from 473 to 673 K, were measured with a Ni–NiCr thermocouple and regulated to within 1 K (see Ref. [15]). A pressure of 50 MPa was applied to all experiments by pumping either argon or water into the vessel. The experiments were finally quenched and both gas and solid analyzed.

2.2.3. Strategy to evaluate the H_2 permeability of the gold sample container

Gas production can be dramatically underestimated if the gold capsule is permeable to hydrogen at the run conditions. Therefore, the permeability of the gold sample container to hydrogen was evaluated by conducting similar hydrothermal experiments but with oxalic acid ($C_2O_4H_2$) as starting material. At temperature above 443 K, oxalic acid decomposes as follows [16]:

$$C_2O_4H_2 \rightarrow CO_2 + H_2O + CO \quad (1)$$

The components produced by this reaction can then react together to various extents depending on run duration and temperature according to the two following reactions:

$$H_2O + CO = H_2 + CO_2 \quad (2)$$

and

$$2H_2 + 2CO = CH_4 + CO_2\,. \quad (3)$$

Following (1), (2) and (3), the number of moles of hydrogen produced during the decomposition of oxalic acid can be deduced from the measurement of the other gas components as follows:

$$n_{H_2C} = \left(n_{CO_2} - n_{CO} - 5n_{CH_4}/2\right) \quad (4)$$

where n_{H_2C} is the calculated number H_2 moles and n_{CO_2}, n_{CO} and n_{CH_4} are the measured number of moles of CO_2, CO and CH_4, respectively.

Table 1 – Experimental conditions, magnetic properties and quantities of produced gases.

Run n°	Reactant	M reactant	M water	Temperature	Duration	Jrs/Js	Hcr/Hc	Js	M magnetite	H_2 MAG	H_2 GC	CH_4	CO_2
		mg	mg	K	h			$\mu A\ m^2$	wt.%	mol/kg	mol/kg	10^{-4} mol/kg	
Initial powder	CBOF					0.050	7.14	102.6	2.21				
COLAC2	CBOF	74.2	80.4	573	162.7	0.219	2.09	436.9	11.25	0.362	0.358	0.705	x
COLAC3	CBOF	102.6	20.0	573	216.0	0.235	1.96	556.6	13.29	0.450	0.393	1.470	
COLAC4	CBOF	84.8	40.3	523	70.4	0.183	2.60	291.2	7.32	0.192	0.167	n.d.	
COLAC5	CBOF	77.6	80.7	523	70.4	0.178	2.68	281.8	6.48	0.156	0.189	n.d.	
COLAC6	CBOF	47.9	119.6	523	70.4	0.176	2.61	205.7	7.06	0.181	0.220	n.d.	
COLAC7	CBOF	41.6	231.3	523	142.8	0.171	2.63	208.5	7.69	0.208	0.174	n.d.	
COLAC8	CBOF	81.9	80.6	523	1362.0	0.200	2.19	412.0	12.5	0.416	0.484	n.d.	
COLAC9	CBOF	81.4	80.5	523	329.3	0.159	2.70	511.9	9.01	0.265	0.229	n.d.	
COLAC10	CBOF	81.6	80.3	623	65.3	0.213	2.09	439.8	10.9	0.346	0.254	0.962	
COLAC11	CBOF	85.9	80.6	473	497.0	0.178	3.01	223.9	5.59	0.117	0.214	n.d.	
COLAC12	CBOF	94.0	80.4	673	43.2	0.213	2.26	497.0	9.77	0.298	0.323	5.342	
COLAC14	CBOF	83.6	80.7	523	785.7	0.218	2.20	481.8	9.54	0.288	0.323	0.717	
COLAC15	CBOF	81.1	80.3	573	66.0	0.189	2.47	238.9	7.59	0.203	0.215	0.296	
COLAC17	CBOF	81.1	81.0	473	69.2	0.098	4.10	237.9	5.49	0.113	0.105	0.167	
COLAC18	CBOF	80.6	80.4	673	68.3	0.224	2.14	420.0	10.10	0.312	0.265	3.376	
OL2C1	BOF	81.33	80.62	673	68.3	0.249	1.99	307.0	8.17	0.229	0.124	1.242	
OL2C2	BOF	86	80.2	523	690.1	0.250	2.11	275.8	5.46	0.111	0.206	n.d.	
Initial powder	CARBOF					0.064	5.74	64.9	1.28				
COLACE11	CARBOF	95.49	14.98	473	167.6	0.156	2.49	274.5	5.39	0.023	0.027	3.399	x
COLACE12	CARBOF	63.33	60.27	573	141.1	0.222	2.12	234.8	9.73	0.210	0.141	3.059	x
COLACE14	CARBOF	40.93	110.9	523	142.8	0.200	2.21	175.9	7.60	0.118	0.102	1.753	
COLACE16	CARBOF	78.45	40.06	523	142.8	0.198	2.26	354.1	6.68	0.079	0.074	1.489	
COLACE17	CARBOF	79.1	80.03	523	1362.0	0.201	2.27	359.0	8.91	0.175	0.171	1.663	
COLACE18	CARBOF	81.12	80.29	523	329.3	0.169	2.52	357.4	7.65	0.121	0.086	1.391	
COLACE19	CARBOF	80.12	80.3	623	65.3	0.214	2.16	450.1	9.07	0.182	0.181	2.137	
COLACE110	CARBOF	79.65	80.59	473	497.0	0.179	2.54	287.9	6.22	0.059	0.078	0.890	
COLACE111	CARBOF	80.17	80.31	673	43.2	0.221	2.33	456.1	9.67	0.208	0.213	6.025	
COLACE112	CARBOF	80.96	80.11	523	785.7	0.205	2.31	326.1	7.54	0.116	0.203	1.981	
COLACE114	CARBOF	82.48	80.32	573	66.0	0.198	2.38	272.2	7.37	0.118	0.095	0.830	
COLACE115	CARBOF	84.02	80.25	673	66.2	0.200	2.31	535.9	12.95	0.349	0.206	3.860	x
COLACE116	CARBOF	82.26	80.2	473	69.2	0.118	3.17	164.6	4.02	0.000	0.001	n.d.	

M reactant, initial mass of reactant; M water, initial mass of water; Jrs, saturation remanent magnetization; Js, saturation magnetization; Hcr, remanent coercivity; Hc, intrinsic coercivity; M magnetite, total mass of produced magnetite; H_2 MAG, amount of hydrogen produced deduced from the magnetic measurement; H_2 GC, amount of hydrogen produced deduced from gas chromatography; CH_4, amount of methane produced deduced from gas chromatography measurement; CO_2, detection of carbon dioxide with gas chromatography.

2.3. Analytical methods

The amount of produced hydrogen was measured by gas chromatography on the recovered gas. The mineralogical evolution of the slag was investigated using quantitative X-ray powder diffraction along with a novel magnetic method [17,18]. From this evolution, the amount of ferrous iron converted into ferric iron was derived since this parameter is expected to be proportional to the amount of produced hydrogen.

2.3.1. Gas analysis

Gas sampling for gas chromatography (GC) analysis was achieved by placing the gold capsule in a syringe equipped with an indenter and a three-way tap (Fig. 1a). We used a Clarus 500 gas chromatograph (PerkinElmer®) equipped with a thermal conductivity detector. The syringe was filled with the same gas as the gas carrier of the GC (Ar, 99.995%). Before piercing the capsule, a blank measurement was carried out on Ar injected in the syringe (Fig. 1b). Then, the capsule was pierced and the experimental gas produced released in the syringe (Fig. 1c). The gas mixture (argon + sampled gas) was sampled through the septum placed on one way of the tap (Fig. 1d) and analyzed by GC. This latter procedure was repeated three times to verify the homogeneity of the gas mixture and the reproducibility of the measurement.

2.3.2. Solid characterization

The recovered solid products were first dried for 48 h in air at 353 K. Then, part of the sample powder was mounted on a double-sided carbon tape and characterized by field emission SEM (Zeiss-Σigma™ equipped with a 50 mm^2 EDS detector; X-Max™ from Oxford Instrument, Ecole normale supérieure, Paris). Another part of the run products was embedded in epoxy and polished for mineral chemistry characterization with FE-SEM, SEM (Hitachi S2500, ISTerre, Grenoble) and electron microprobe (Cameca SX100, Camparis, Paris). The powders were also analyzed by XRPD with a Bruker D5000 or D8 diffractometer (ISTerre). The instruments were operating with CuKα radiation, step size of 0.026° 2θ and a counting parameter of 8 s. The divergence slit, the anti-scatter slit, and detector slit were 1, 1, 0.2 mm, respectively. The X-ray patterns were analyzed with Rietveld using the BGMN software [19]. Portlandite, magnetite, wüstite, calcite, lime and α-ferrite were refined using the internal structure database of BGMN whereas the crystal structures given by [20–22] were used for larnite, brownmillerite and hibschite, respectively.

The amount of magnetite produced by ferrous iron oxidation was estimated from the saturation magnetization (Js) of the sample [17] which is directly proportional to the quantity of magnetite. At the end of the experiments, the solid products were firmly packed in non-magnetic capsules which were placed in a Princeton Micromag Vibrating Sample Magnetometer 3900 at (IPGP, Paris) for Js measurements. A proportionality factor of 92 A m^2/kg was used to convert the Js signal into a quantity of magnetite [17].

3. Results

3.1. Mineralogical composition of the starting slag materials

The main mineral constituents of the CBOF powder (proportions are given in Table 2) are:

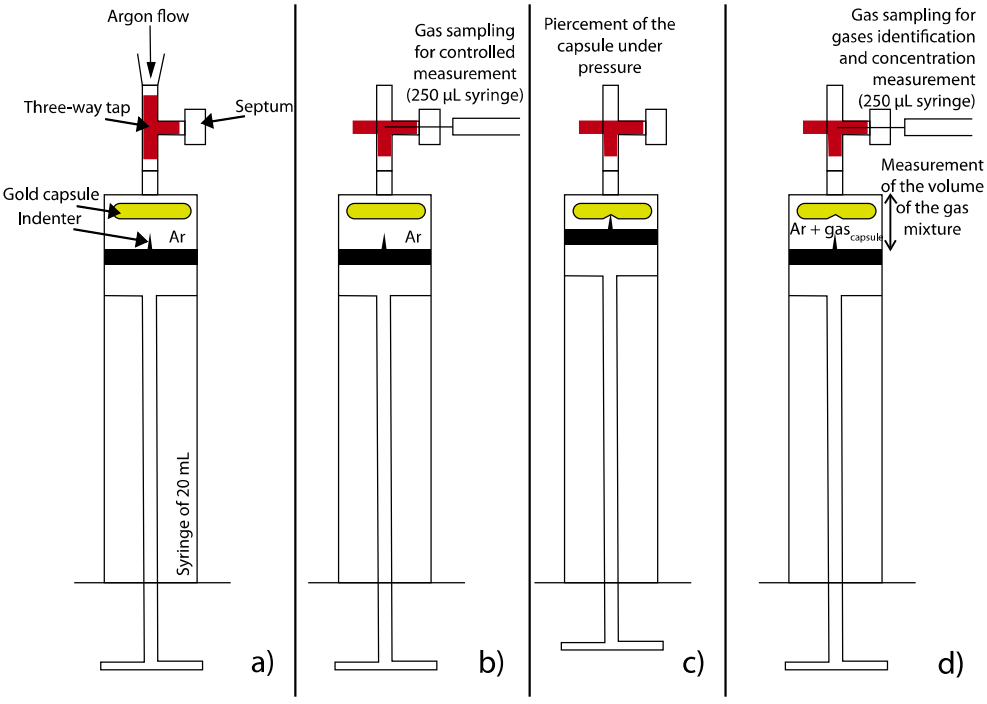

Fig. 1 – Sketch of the gas sampling set-up. a: the syringe of 20 mL is filled with the gold capsule and argon. b: a controlled measurement is made by sampling the gas in the closed 20 mL syringe with a 250 µL syringe through the septum. c: the gold capsule is pierced by using an indenter. d: the volume and the composition of the gas in the 20 mL syringe are measured.

Table 2 — Results of the rietveld analysis.

Run no	Reactant	Portlandite	Magnetite	Wüstite	Larnite	Calcite	Brownmillerite	Lime	Aragonite	Iron	Hibschite	Fe^{3+}/Fe_{tot}
		$Ca(OH)_2$	Fe_3O_4	$(Fe_{0.60},Mn_{0.08},Mg_{0.30},Ca_{0.02})O$	$9{\cdot}Ca_2SiO_4 + 1Ca_3(PO_4)_2$	$CaCO_3$	$Ca_2(Al_{0.36},Fe_{1.28},Ti_{0.23})O_{4.9}$	$(Ca_{0.92}Mn_{0.03}\ Fe_{0.05})O$	$CaCO_3$	Fe	$Ca_3Al_{1.4}Fe_{0.6}(SiO_4)_2(OH)_4$	
		wt.%	wt.%	wt.%	wt.%	wt.%	wt.%	wt.%	wt.%	wt.%	wt.%	Mole fraction
Initial powder	CBOF	11.0	0.6	24.0	25.8	3.3	16.4	7.2	10.9	0.7	0.1	0.27
COLAC2	CBOF	22.5	11.2	8.5	11.8	10.5	12.2	1.7	0	0.4	21.2	0.55
COLAC3	CBOF	24.8	14.7	6.3	8.7	13.2	8.9	0.2	0	0.3	22.9	0.59
COLAC4	CBOF	24.9	6.2	11.4	9.3	13.5	6.8	0.3	0	0.5	27.0	0.41
COLAC5	CBOF	20.7	5.4	15.4	10.6	12.8	12.6	0.4	0	0.7	21.3	0.40
COLAC6	CBOF	21.1	6.0	15.7	9.9	12.3	12.5	0.6	0	0.8	21.1	0.40
COLAC7	CBOF	18.2	6.3	23.8	9.5	11.0	11.4	0.2	0	1.0	18.7	0.31
COLAC8	CBOF	23.6	10.6	8.1	10.0	13.9	6.7	0.7	0	0.3	26.0	0.52
COLAC9	CBOF	24.9	7.0	16.0	9.2	11.7	11.0	0.4	0	0.6	19.3	0.40
COLAC10	CBOF	20.5	10.6	11.6	10.3	12.1	10.8	0.1	0	0.3	23.6	0.49
COLAC11	CBOF	22.2	4.3	13.5	10.5	12.3	7.3	0.4	0	0.5	28.9	0.36
COLAC12	CBOF	23.1	11.1	12.8	9.0	12.3	11.7	0.1	0	0.2	19.6	0.48
COLAC14	CBOF	24.1	9.6	7.9	8.8	12.1	7.8	0.5	0	0.3	28.9	0.53
COLAC15	CBOF	22.6	7.0	12.2	9.1	13.2	8.3	0.9	0	0.4	26.3	0.43
COLAC17	CBOF	23.5	2.9	13.5	7.3	13.1	7.0	0.5	0	0.4	31.8	0.34
COLAC18	CBOF	22.0	11.8	12.3	7.0	13.8	11.9	0.1	0	0.2	20.8	0.50
OL2C1	BOF	34.6	10.6	16.1	11.7	3.9	8.1	4.0	0	0.4	10.5	0.40
OL2C2	BOF	37.2	6.0	13.3	2.3	4.8	19.3	0.5	0	0.2	16.3	0.50
Initial powder	CARBOF	0	1.1	19.7	8.6	48.6	12.6	0.7	3.1	0.8	5.0	0.28
COLACE11	CARBOF	0	4.4	21.4	10.1	34.7	5.3	0.4	0	0.6	23.1	0.25
COLACE12	CARBOF	0	10.4	11.8	7.9	39.9	5.0	0.2	0	0.2	24.5	0.45
COLACE14	CARBOF	0	7.8	16.1	8.9	37.1	4.7	0.3	0	0.4	24.8	0.35
COLACE16	CARBOF	0	7.4	14.2	9.6	36.2	6.5	0.3	0	0.5	25.3	0.39
COLACE17	CARBOF	0	10.9	16.4	4.2	45.8	3.8	0.2	0	0.4	18.3	0.37
COLACE18	CARBOF	0	8.0	18.0	10.6	43.7	3.2	0.5	0	0.5	15.7	0.30
COLACE19	CARBOF	0	10.1	16.4	7.8	38.6	7.3	0.2	0	0.1	19.5	0.40
COLACE110	CARBOF	0	5.8	15.9	7.3	44.3	4.7	0.3	0	0.3	21.5	0.32
COLACE111	CARBOF	0	10.6	15.0	9.5	40.3	8.0	0.3	0	0.2	16.1	0.42
COLACE112	CARBOF	0	7.3	13.7	7.5	41.3	4.3	0.3	0	0.2	25.4	0.37
COLACE114	CARBOF	0	7.0	15.7	8.1	39.5	6.0	0.5	0	0.3	22.8	0.36
COLACE115	CARBOF	0	10.9	18.4	8.5	37.3	11.3	0.4	0	0.1	13.2	0.41
COLACE116	CARBOF	0	3.3	16.7	8.9	40.7	5.1	0.3	0	0.4	24.5	0.27

larnite (Ca_2SiO_4) with up to 2 wt.% of FeO and in solid solution with approximately 10 mol.% $Ca_3(PO_4)_2$. This phase is referred to as P–larnite in the following.
- a mixture between brownmillerite, $Ca_2(Al,Fe^{3+})_2O_5$, and perovskite ($CaTiO_3$) referred to as Ti–brownmillerite.
- a (Fe,Mg,Mn,Ca)-oxide referred to as Mg–wüstite.
- lime (CaO) containing up to 10 wt.% of FeO and MnO along with portlandite, $Ca(OH)_2$, and calcium carbonates (calcite and aragonite) resulting from the atmospheric hydration and carbonation of lime, respectively.

Ferrite (Fe) was also detected with SEM and X-ray powder diffraction.

In comparison, CARBOF powder contains less P–larnite, Ti–brownmillerite and Mg–wüstite. Lime and aragonite were not observed and calcite occurred as the single carbonate. Additionally, a calcic hydrogarnet (hibschite) was also detected in the CARBOF starting material.

In all the run products (i.e. with CBOF or CARBOF as starting materials), an iron oxide was observed under the SEM (Fig. 2). X-ray diffraction and the low coercivity of the samples, which saturate by 300 mT, indicated that this iron oxide was magnetite. SEM and EDS analyses showed the presence of a rhombohedral calcium rich phase (Fig. 2). Furthermore, TGA display a weight loss of around 12% between 973 and 1073 K (Fig. 3). These two latter results are indicative of the occurrence of calcite which was also detected with X-ray diffraction.

The amount of carbonate formed during the carbonation experiments was estimated by using both the pressure drop associated with carbonate formation (P_{seq}) and TGA data. P_{seq} after 6 days of experiments was of 1.25 ± 0.5 bar. This corresponds to a sequestration of 0.112 ± 0.044 kg of CO_2 per kg of steel slag. TGA data indicated that CO_2 degassing associated with thermal decarbonation accounts for a weight loss of 0.810 wt.% in CBOF and of 13.1 wt.% in CARBOF. The conversion of these values into a quantity of sequestered CO_2 during the experiment yields an uptake of 0.142 ± 0.002 kg of CO_2 per kg of steel slag. This result is consistent, within uncertainty, to the estimate using P_{seq}. Carbonation induces a pH drop from 12.67 (CBOF) down to 6.86 (CARBOF), as measured at 298 K.

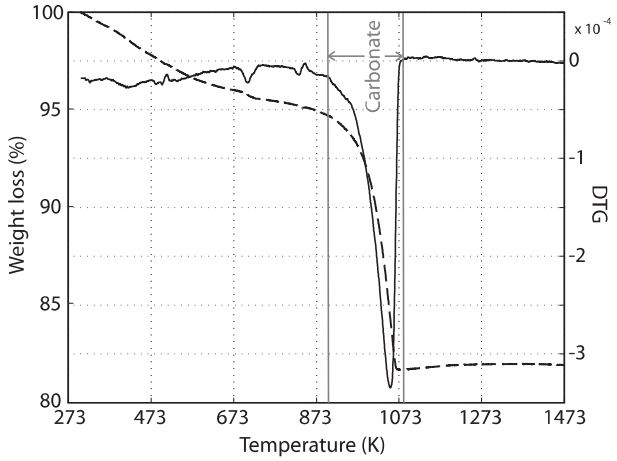

Fig. 3 – Thermogravimetric (dashed line) and derivative thermogravimetric (DTG; plain line) analyses of the carbonated BOF steel slag.

3.2. Gold permeability with respect to H_2

As shown by Ref. [23], permeability of gold with respect to hydrogen mainly depends on temperature and hydrogen fugacity gradient. We investigated semi-quantitatively gold permeability by measuring the leakage of H_2 produced by the decomposition of oxalic acid contained in a gold capsule (Fig. 4). After 150 h, a hydrogen leakage of 5, 60 and 70% occurred at temperatures of 473, 573 and 623 K, respectively. This result suggests that hydrogen did not significantly permeate in experiments conducted at temperature below 573 K. Moreover, at 623 K, hydrogen leakage stabilized at a value of 70 ± 15%, i.e. for approximately 3×10^{-5} mol of hydrogen remaining in the capsule. This value can be converted into a given fH_2 and fH_2 gradient if external fH_2 is considered as negligible. In conclusion, hydrogen leakage through the walls of our gold capsules is only significant at temperatures above 623 K and/or when the hydrogen content exceeds approximately 3×10^{-5} mol in the capsule.

3.3. Chemical and mineralogical evolution of the BOF slag

3.3.1. Mineralogical evolution of the solid phases and iron redistribution

The mineralogical evolution of the slag (Table 2) can be summarized as follows: The Ti–brownmillerite content decreased whereas the hibschite content increased from below detection

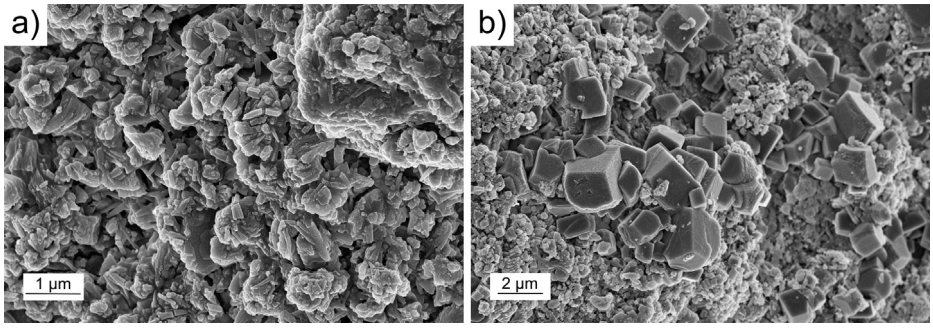

Fig. 2 – SEM images of the surface of CBOF (a) and CARBOF (b) powders showing the formation of rhombohedral calcite in CARBOF.

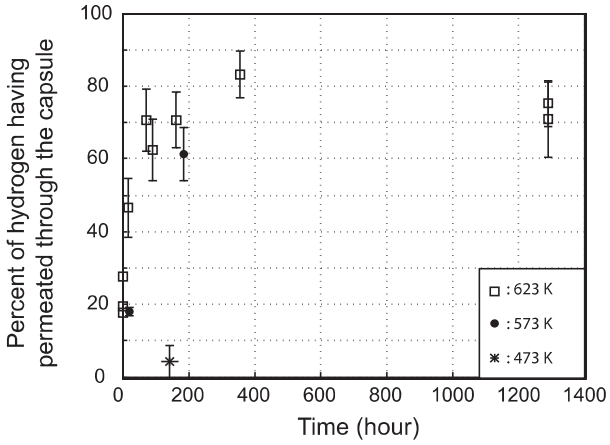

Fig. 4 – Percentage of hydrogen having permeated through gold as a function of time in experiments on acid oxalic decomposition at three different temperatures. Note that at least 20% of the initial hydrogen remained after 1300 h in the gold capsule at 350 °C.

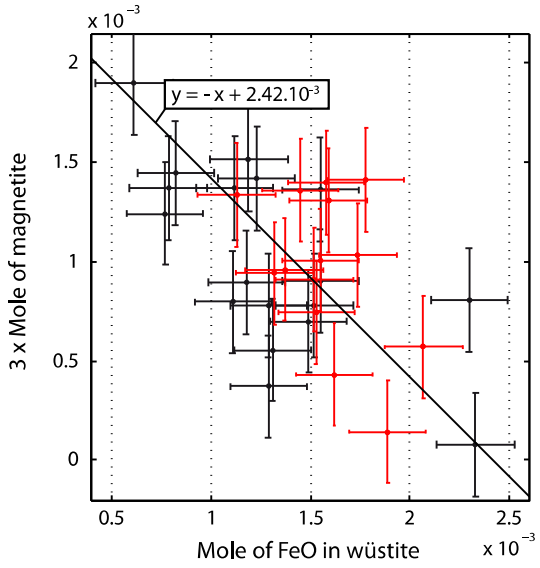

Fig. 5 – Magnetite content as a function of wüstite content both derived from Rietveld analyses in all the reaction products. The experiments on hydrogen production using BOF/CBOF are in black and CARBOF in red. Note that the magnetite content increases as the wüstite content decreases in a three to one ratio suggesting that wüstite oxidation is by far the main reaction producing magnetite in our experiments. (For interpretation of the references to colour in this Figure legend, the reader is referred to the web version of this article.)

limit in CBOF and 5 wt.% in CARBOF to an average value, on all the performed experiments, of 22 wt.%. The total ferric iron contained in these two minerals was rather constant with values of $8.1 \times 10^{-4} \pm 0.7 \times 10^{-4}$ and $5.8 \times 10^{-4} \pm 1.0 \times 10^{-4}$ mol per g of powder in the CBOF and CARBOF experiments, respectively. This result suggests that hibschite formed at the expense of Ti–brownmillerite and that, therefore, hibschite formation was not the product of an oxidation reaction.

P–larnite content decreases from 26 wt.% in the CBOF powder to 8.8 ± 1.9 wt.% in all the experiments whatever their duration and even in the carbonation experiments performed at ambient temperature. Apparently, P–larnite reacted at the early stage of the hydrothermal treatment. P–larnite contained up to 2 wt.% of ferrous iron that could have been oxidized during this early stage.

Mg–wüstite content was found to decrease whereas magnetite content increased in the course of the hydrothermal process. These variations appear to be proportional as shown in Fig. 5. For example, the concentration in Mg–wüstite decreased from 24 ± 2 wt.% to 6 ± 2 wt.% whereas the magnetite content increased from 1 ± 2 wt.% to 15 ± 2 wt.% in COLAC3 (Table 2). Magnetic measurements also attested for a strong increase in the magnetite content in all experiments (Table 1). Texturally, magnetite seems to grow at the expense of Mg–wüstite since it is found to rim Mg–wüstite grains (Fig. 6). It can be inferred from these results that the main magnetite forming reaction is the oxidation of wüstite:

$$3FeO + H_2O = Fe_3O_4 + H_2 \quad (5)$$

In the experiments using CBOF as starting material, lime was hydrated into portlandite. Since lime contained 5 mol.% of FeO, this hydration reaction induced the oxidation of ferrous iron in the system following Eq. (5). The disappearance of ferrite is likely due to its oxidation into magnetite. However, with an initial abundance of less than 2%, ferrite oxidation cannot contribute significantly to the total amount of produced magnetite.

3.3.2. *Gaseous phase chemistry*

H_2 was produced in all experiments. Up to 0.42 and 0.32 mol of H_2 per kg of reactant was produced in COLAC8 and COLAC12 at 523 and 673 K for 1362 and 43 h, respectively. CH_4 was detected in all CARBOF experiments but COLACE116, with an average molar CH_4/H_2 ratio of ca. 0.016.

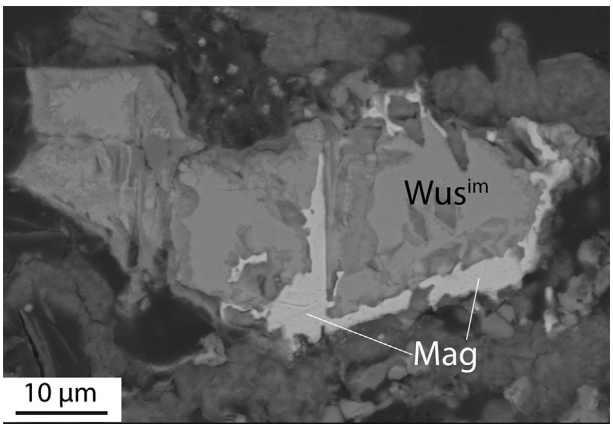

Fig. 6 – Backscattered electron image of a wüstite grain partially replaced at its rim by magnetite (run COLAC2).

In BOF and CBOF, CH_4 production is one to two orders of magnitude lower and the averaged CH_4/H_2 ratio increases from 7×10^{-5} at 473 K to 1.3×10^{-3} at 673 K (Fig. 7).

Concentrations of CO_2 close to the detection limit of the GC were also detected in one CBOF experiment and in three CARBOF experiments (Table 1).

3.3.3. *Chemical reaction of H_2 production*

Fig. 8 shows that hydrogen production is clearly correlated with Fe^{2+} to Fe^{3+} oxidation in the powder. The main Fe^{3+}-bearing phase that was produced during the experiments is magnetite which can be precisely quantified by magnetic measurements [17]. As shown above, magnetite was mainly produced through the oxidation of wüstite. Eq. (5) shows that 1 mol of hydrogen should be produced per mole of magnetite. This mass balance relationship is verified in all experiments, i.e. either BOF/CBOF or CARBOF (Fig. 9). H_2 production results directly from the oxidation of wüstite according to Eq. (5). Furthermore, Fig. 9 shows that significant magnetite can form without producing hydrogen at the beginning of the hydrothermal treatment. Magnetite formed at this stage is probably the result of wüstite oxidation by the dioxygen initially present in the capsule (air contamination and O_2 dissolved in the water loaded in the capsule), preliminary to H_2 production, as followed:

$$6FeO + O_2 = 2Fe_3O_4 \quad (6)$$

3.4. *Kinetics of hydrogen production*

In the following section, kinetics of H_2 production were quantified by using reaction progresses as a function of time. The reaction progresses were calculated as percentages of the total amounts of hydrogen that BOF or CARBOF steel slag can produce. These amounts were estimated by using Eq. (5) and the initial amount of FeO contained in the reactants.

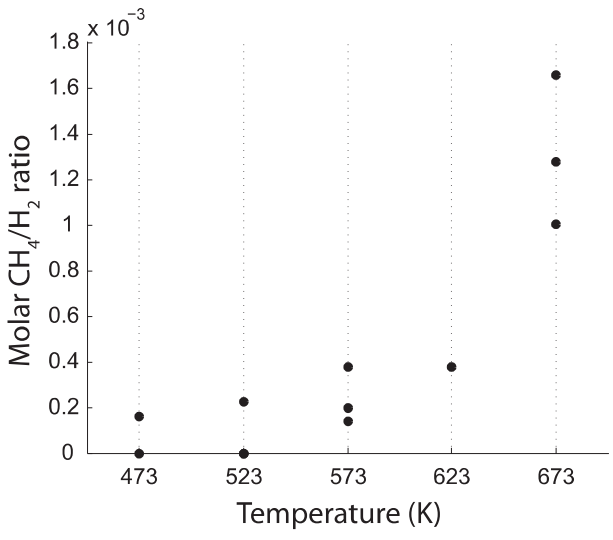

Fig. 7 – CH_4/H_2 ratio as a function of temperature in experiments using CBOF powder as starting material.

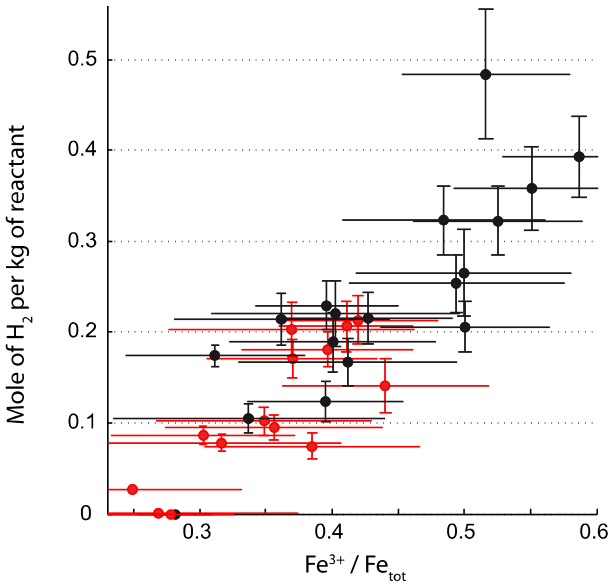

Fig. 8 – Relationship between the quantity of produced hydrogen and the Fe^{3+}/Fe_{tot} ratio in the powder, derived from the Rietveld analysis and the average composition of the phases. The experiments using CBOF and CARBOF as starting materials are in black and red, respectively. (For interpretation of the references to colour in this Figure legend, the reader is referred to the web version of this article.)

3.4.1. *Kinetics of hydrogen production at 523 K/50 MPa*

The hydrogen production rate with CBOF plotted as a function of time shows two regimes (Fig. 10). First, very high kinetics of hydrogen production are observed below 50 h (15–20% of reaction progress with a production rate of 0.4%/h). This stage is interpreted as resulting from the fast reaction of small wüstite

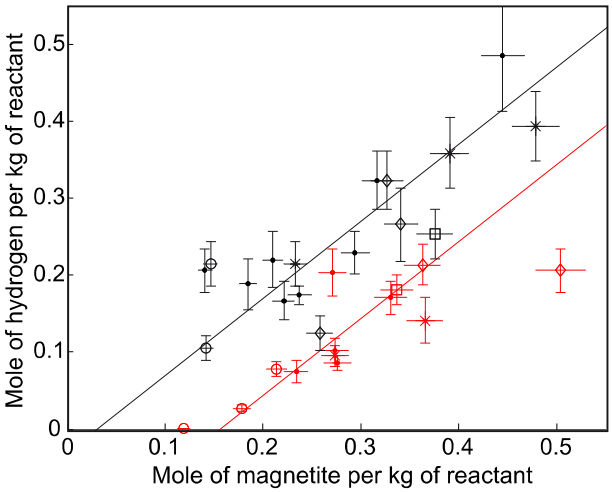

Fig. 9 – Relationship between the quantities of magnetite and hydrogen (estimated using magnetism and chromatography, respectively) produced in experiments using BOF/CBOF (black) and CARBOF (red) as starting materials. (For interpretation of the references to colour in this Figure legend, the reader is referred to the web version of this article.)

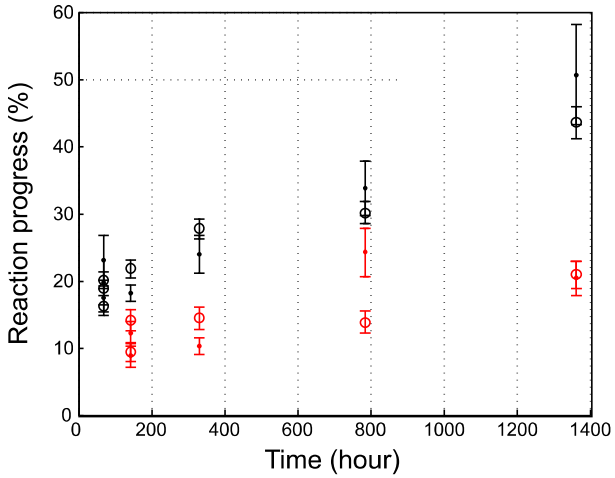

Fig. 10 – Reaction progress as a function of time for experiments conducted at 523 K with CBOF (black) and CARBOF (red) powders as starting materials. The reaction progress was calculated from the initial content of FeO in the powders and either the amount of produced hydrogen (dots) or the amount of produced magnetite (open circles). (For interpretation of the references to colour in this Figure legend, the reader is referred to the web version of this article.)

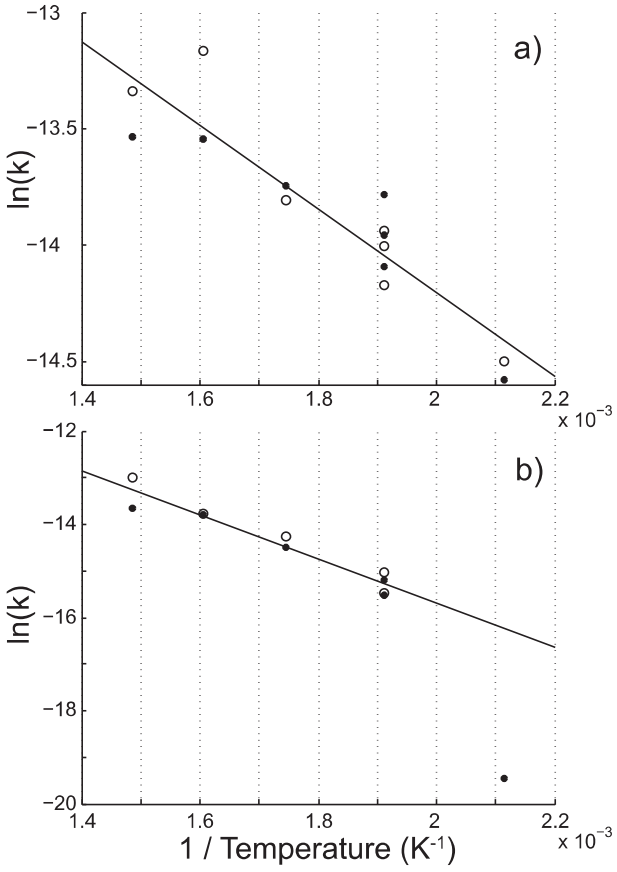

Fig. 11 – Arrhenius plots of the kinetic constant for the experiments using CBOF (a) or CARBOF (b) as starting materials. The constants of the reaction (5) (k in s^{-1}) were determined by fitting a first order kinetics to the reaction progress vs. time curves. The reaction progresses were derived from the amount of produced hydrogen (dots) or from the amount of produced magnetite (open circle). The plain lines are the fits used to derive the activation energies. For experiments using CARBOF as starting material (b), the experiment at 473 K (COLACE116) was not used for the fit because its reaction progress is close to zero and its error has too much weight on the derived activation energy value.

grains, lime, ferrite and part of P–larnite (Table 2). These compounds contain Fe^0 or Fe^{2+} which are oxidized and incorporated into magnetite. Then, the production rate of hydrogen decreases down to approximately 0.024%/h. This stage corresponds to the oxidation of Mg–wüstite into magnetite according to reaction Eq. (5).

3.4.2. *Influence of the initial particle size*

The influence of the initial particle size (IPS) on the kinetics of hydrogen production can be evaluated by comparing experiments using BOF as starting material (OL2C1 and OL2C2; IPS < 4 mm) with experiments using CBOF (COLAC14 and COLAC18; IPS < 50 μm). At 523 K after about 700 h, the reaction progress reached 17% with BOF and 28% with CBOF. At 673 K after 68 h, reaction progress reached 24% in BOF and 33% in CBOF. Overall, crushing is found to increase the H_2 production kinetics by a factor of 1.4–1.7 only.

3.4.3. *Influence of the temperature*

After about 70 h, the reaction progress reached 10% at 473 K whereas it reached 32% at 673 K suggesting that the reaction is thermally activated. Assuming first-order kinetics, the retrieved kinetic constants display an Arrhenius behaviour with an activation energy for the hydrogen production reaction(s) of 15 ± 2 kJ/mol (Fig. 11).

3.4.4. *Influence of the pH through preliminary carbonation*

The two regimes of hydrogen production rate observed for the CBOF powders were also observed for CARBOF (Fig. 10). However, half as hydrogen was produced during the first stage and the reaction kinetics in the second stage were three times lower with CARBOF than with CBOF at 523 K. On the contrary, after 67 h at 673 K, the reaction progress with CARBOF (40%) exceeded that of CBOF (32%). Still assuming a first order kinetics, the activation energy (Ea) of the hydrogen production with CARBOF of 41 ± 12 kJ/mol is derived (Fig. 11), which is 2.7 times higher than the Ea inferred for the CBOF powder. Thus, the production of hydrogen could potentially become more efficient with carbonated steel slags for temperature above 673 K.

4. Discussion

4.1. *Hydrogen production inferred from the magnetic data*

H_2 permeability experiments with oxalic acid showed that hydrogen must not have significantly leaked in the course of

our experiments which have been performed at temperatures below 573 K and/or with hydrogen production below 3×10^{-5} mol of H_2. The production of hydrogen is proportional to the production of magnetite, the amount of which can be measured through magnetic measurements. Both GC and magnetic determinations of the hydrogen production are consistent (Fig. 9) and the magnetic tool is therefore suitable for estimating hydrogen production. Conversely, a comparison between GC and magnetic data allows determining the amplitude of H_2 leakage which is significant for only three high temperature experiments (COLAC10 at 623 K and OL2C1 and COLACE115 at 673 K).

4.2. *Economically relevant parameters for hydrogen production from steel slags*

Crushing led to a particle size reduction by a factor of 80. Assuming that (1) reaction kinetics are controlled by the dissolution of wüstite and thus proportional to the reactive surface area and that (2) the reactive surface area of the slag material is proportional to the particle surface area, hydrogen production reaction kinetics should have increased by about three orders of magnitude after crushing. Crushing actually led to a limited reaction kinetics enhancement, by a factor of 1.4–1.7 only. Either the kinetics of the reaction were not dependent on the wüstite surface area [18] or the reactive surface area of the BOF steel slag was not significantly increased by crushing. Particles are actually not single mineral grains but they rather represent high porosity aggregates as suggested by BET surface area measurements [11]. Anyway, regarding the cost of crushing at the industrial scale, this operation appears irrelevant.

The method allows the production of 0.2 mol (or 4.5 L at 293 K and 0.1 MPa, i.e. NL) of hydrogen per kg of slag at 523 K in 70 h. High-purity hydrogen can be recovered after removing steam from the gas by condensation. The purity of hydrogen produced at 523 K and calculated as the volume ratio $H_2/(H_2 + CH_4 + CO + CO_2)$ is of 99.995% (equivalent to grade C following ISO 14687 norms). The production can be increased by a factor of three by running the experiment at a temperature of 673 K instead of 473 K. Besides the energy cost of increasing the process temperature, methane production will also be increased by one to two orders of magnitude. At 673 K, after water removal, the hydrogen purity is expected to reach values higher than 99.9% (equivalent to grade B).

Ref. [24] has shown that the dissolution rate of wüstite decreases with pH in acidic conditions at 298 K. In our experiments, by comparing carbonated and uncarbonated BOF steel slags, lowering the pH from basic to neutral is found to result in a lower kinetics of H_2 production below 673 K. These observations are compatible with the often observed U-shaped dependence of the dissolution rate of minerals on pH [25,26]. The lowering of pH associated with the carbonation of steel slags also increases the corrosion of steel in which the reactor for H_2 production may be made at industrial scale [27]. However, this corrosion is expected to be limited since the oxygen activity, the main contributor to the corrosion of steel [27], is very low in our H_2 producing experiments. The high performance of BOF steel slag regarding carbonation [9,11] was confirmed here with a sequestration of 0.142 ± 0.002 kg of CO_2 per kg of steel slag at a P_{CO_2} of 2 MPa. Moreover, these carbonated materials produce CH_4 in concentrations by one to two orders of magnitude higher. The formation of CH_4 is due to the reaction between H_2 and CO_2 which occurs during the thermal breakdown of carbonates, in particular that of ferrous carbonates [28,29]; hydrogen of lower purity is then obtained (purity above 98%, equivalent to grade A).

All experiments were conducted at 50 MPa in order to prevent capsule damage due to the internal volume increase caused by gas production and H_2O expansion. Industrial processes can hardly be conducted at such high pressure. However, pressure has little effect on the kinetics of hydrothermal reactions in comparison to temperature and pH. It is thus expected that working at vapour pressure (4 MPa at 523 K) or slightly above should yield comparable rates of hydrogen production.

4.3. *Rate of ferrous iron conversion and efficiency of hydrogen production with BOF steel slag*

Potentially, the reaction of all the ferrous iron contained in the BOF steel slag could produce 0.9 mol H_2 or 22 NL per kg. The present study shows that the conversion of ferrous into ferric iron increases with temperature and run duration. At 523 K and after 70 h, the amount of conversion was about 20% and, for the longest experiment (1360 h at 523 K) or at 673 K after 70 h, amounts of conversion of 40–50% were reached. There is consequently a potential for increasing H_2 production by a factor of about two.

The required energy to heat the slag adiabatically from 298 to 523 K is 200 kJ/kg. This energy can be compared to the energy that can be recovered from the produced hydrogen at the same temperature (approximately 0.2 mol/kg, i.e. 50 kJ/kg). Thus, the efficiency of this method is of ca. 25% at 523 K considering only the energy required for heating the slag. This efficiency falls in the range of other production methods which have typical efficiencies comprised between 9 and 85% with the highest efficiency attained with steam reforming [30]. The efficiency can be improved if higher conversion is reached or if the heat associated with lime hydration (about 300 kJ/kg of slag) is recovered.

4.4. *Generalization of the method to other wastes*

The method proposed here is based on the reaction of BOF steel slags in hydrothermal conditions to produce hydrogen. The potential of these slags for producing hydrogen relies on their high content in ferrous iron. Among other steel slags, electric arc furnace (EAF) steel slags contain up to 70 wt.% of magnesio-wüstite and 25 wt.% of FeO on average [31]. They are consequently good candidates for hydrogen production as well. Among the other waste forms, slags produced in municipal waste incinerator contain on average 7 wt.% of Fe. In order to estimate their potential for hydrogen production, the oxidation state of iron and the phases containing this element (wüstite is typically not observed in these wastes) should be investigated.

5. Conclusions

1. We document here that the hydrothermal treatment of steel slags at relatively low temperature (<773 K) induces oxidation reactions with a simultaneous reduction of water. This reaction produced magnetite and hydrogen.
2. High purity hydrogen can be formed with this process (grade C, above 99.995% of purity).
3. We developed a characterization protocol to monitor hydrogen produced in sealed gold capsules with combines GC and magnetic measurements. Due to its accuracy and simplicity, magnetic measurement could be used for estimating hydrogen production in similar iron-bearing waste systems.
4. The steel slag can be carbonated beforehand to sequester 0.142 ± 0.002 kg of CO_2 per kg of slag. However, slag carbonation reduces the kinetics of hydrogen production at temperature below 673 K and leads to the production of higher amounts of CH_4.
5. By producing hydrogen and allowing CO_2 sequestration, this method increases the value of a material considered as a waste. Moreover, it has efficiency comparable to the efficiency of the other processes dedicated to hydrogen production.
6. This method can certainly also be used to produce hydrogen with EAF steel slag. The sum of the annual productions of BOF and EAF steel slags in Europe, USA, China and Japan is of 47 million of tons [32]. Considering a total conversion of these steel slags (0.9 mol (or 22 NL) of H_2 per kg), this method has the potential for producing 85,000 tons of hydrogen per year. Nowadays, approximately 2% of the global hydrogen production (i.e. 2% of 69 million of ton per year [33]) is achieved according to processes which do not release CO_2 in the atmosphere (water electrolysis, thermochemical water splitting, thermocatalytic methane decomposition,…). Consequently, the method presented here could supply 5–10% of the annual production of hydrogen produced without CO_2 emission or even with a negative CO_2 balance if slag carbonation is associated with this method.

Acknowledgements

This research was funded by INSU-CNRS through the "Hydrogène Naturel" program. F.B. gratefully acknowledges funding from ISTerre (BQR) for the high-pressure equipment. We are also thankful to the ENS laboratory and Damien Deldicque for SEM access. This is IPGP contribution number 3395.

REFERENCES

[1] Marbán G, Valdés-Solís T. Towards the hydrogen economy? Int J Hydrogen Energ 2007;32:1625–37.
[2] Messerschmitt. Verfahren zur Erzeugung von Wasserstoff durch abwechselnde Oxidation und Reduktion von Eisen in von außen beheizten, in den Heizräumen angeordneten Zersetzern. DE 266863 1911.
[3] Hacker V, Fankhauser R, Faleschini G, Fuchs H, Friedrich K, Muhr M, et al. Hydrogen production by steam–iron process. J Power Sources 2000;6:531–5.
[4] Lorente E, Peña JA, Herguido J. Separation and storage of hydrogen by steam–iron process: effect of added metals upon hydrogen release and stability. J Power Sources 2009;192:224–9.
[5] Chaurand P, Rose J, Bottero J-Y, Domas J. Speciation of Cr and V within BOF steel slag reused in road constructions. J Geochem Explor 2006;88:10–4.
[6] Bhattacharjee D, Mukharjee T, Tathavadkar V. Set-up for production of hydrogen gas by thermo-chemical decomposition of water using steel plant slag and waste materials. United States Patent Application Publication; 2011.
[7] Matsuura H, Tsukihashi F. Thermodynamic calculation of generation of H_2 gas by reaction between FeO in steelmaking slag and water vapor. ISIJ Int 2012;52:1503–12.
[8] Sato M, Matsuura H, Tsukihashi F. Generation behaviour of H_2 gas by reaction between FeO-containing slag and H_2O–Ar gas. ISIJ Int 2012;52:1500–2.
[9] Huijgen WJJ, Witkamp G-J, Comans RNJ. Mineral CO_2 sequestration by steel slag carbonation. Environ Sci Technol 2005;39:9676–82.
[10] Montes-Hernandez G, Pérez-Lopez R, Renard F, Nieto JM, Charlet L. Mineral sequestration of CO_2 by aqueous carbonation of coal combustion fly-ash. J Hazard Mater 2009;161:1347–54.
[11] Chang E-E, Chen C-H, Chan Y-H, Pan S-Y, Chiang P-C. Performance evaluation for carbonation of steel-making slags in a slurry reactor. J Hazard Mater 2011;186:558–64.
[12] Chaurand P, Rose J, Briois V, Salome M, Proux O, Nassif V, et al. New methodological approach for the vanadium K-edge X-ray absorption near-edge structure interpretation: application to the speciation of vanadium in oxide phases from steel slag. J Phys Chem B 2007;111:5101–10.
[13] Chaurand P, Rose J, Briois V, Olivi L, Hazemann J-L, Proux O, et al. Environmental impacts of steel slag reused in road construction: a crystallographic and molecular (XANES) approach. J Hazard Mater 2007;139:537–42.
[14] de Windt L, Chaurand P, Rose J. Kinetics of steel slag leaching: batch tests and modeling. Waste Manage 2011;31:225–35.
[15] Brunet F, Chopin C. Bearthite, $Ca_2Al(PO_4)_2(OH)$: stability, thermodynamic properties and phase relations. Contrib Mineral Petrol 1995;121:258–66.
[16] Javoy M, Pineau F, Iiyama I. Experimental determination of the isotopic fractionation between gaseous CO_2 and carbon dissolved in tholeiitic magma. Contrib Mineral Petrol 1978;67:35–9.
[17] Malvoisin B, Carlut C, Brunet F. Serpentinization of oceanic peridotites: 1. A high-sensitivity method to monitor magnetite production in hydrothermal experiments. J Geophys Res 2012;117:B01104.
[18] Malvoisin B, Brunet F, Carlut C, Rouméjon S, Cannat M. Serpentinization of oceanic peridotites: 2. Kinetics and processes of San Carlos olivine hydrothermal alteration. J Geophys Res 2012;117:B04102.
[19] Taut T, Kleeberg R, Bergmann J. The new Seifert Rietveld program BGMN and its application to quantitative phase analysis. Mater Struc 1998;5:57–66.
[20] Saalfeld H, Klaska KH. The crystal structure of 6 Ca_2SiO_4. 1 $Ca_3(PO_4)_2$. Z für Krist 1981;155:65–73.
[21] Colville AA, Geller S. The crystal structure of brownmillerite, Ca_2FeAlO_5. Acta Crystallogr 1971;B27:2311–5.
[22] Basso R, Giusta AD, Zefiro L. Crystal structure refinement of plazolite: a highly hydrated natural hydrogrossular. Neues Jahrbuch für Mineralogie 1983:251–8.

[23] Chou I-M. Permeability of precious metals to hydrogen at 2 kb total pressure and elevated temperatures. Am J Sci 1986;286:638–58.
[24] Jang J-H, Brantley SL. Investigation of wüstite (FeO) dissolution: implications for reductive dissolution of ferric oxides. Environ Sci Technol 2009;43:1086–90.
[25] Hellmann R. The albite–water system: part I. The kinetics of dissolution as a function of pH at 100, 200, and 300 °C. Geochim Cosmochim Acta 1994;58:595–611.
[26] Oelkers EH. General kinetic description of multioxide silicate mineral and glass dissolution. Geochim Cosmochim Acta 2001;65:3703–19.
[27] Escalante E, Ito S. Measuring the rate of corrosion of steel in concrete. In: Berke NS, Chaker V, Whiting D, editors. Corrosion rates of steel in concrete. ASTM; 1990. p. 86–102.
[28] Marocchi M, Bureau H, Fiquet G, Guyot F. In-situ monitoring of the formation of single-carbon compounds during the dissolution of iron (II) carbonate (siderite). Chem Geol 2011;290:145–55.
[29] McCollom TM. Formation of meteorite hydrocarbons from thermal decomposition of siderite ($FeCO_3$). Geochim Cosmochim Acta 2003;67:311–7.
[30] Holladay JD, Hu J, King DL, Wang Y. An overview of hydrogen production technologies. Catal Today 2009;139:244–60.
[31] Geiseler J. Use of steelworks slags in Europe. Waste Manage 1996;16:59–63.
[32] Shen H, Forssberg E. An overview of recovery of metals from slags. Waste Manage 2003;23:933–49.
[33] Hydrogen production & distribution. IEA energy technology essentials. International Energy Agency; 2007.